RESEARCH ARTICLE

Photocatalytic removal of 17β-estradiol from water using a novel bimetallic NiCu/Nb$_2$O$_5$ catalyst

Ramiro Picoli Nippes[1] · Aline Domingues Gomes[1] · Paula Derksen Macruz[1] · Marcos de Souza[1]

Abstract

The development of effective photocatalytic materials is essential for removing emerging pollutants from aqueous media, such as the hormone 17β-estradiol (E2). In this study, a novel photocatalyst based on niobium pentoxide (Nb$_2$O$_5$) functionalized with nickel (Ni) and copper (Cu) was synthesized for E2 removal. The NiCu/Nb$_2$O$_5$ photocatalyst was prepared using a facile wet impregnation method and characterized by various techniques. The incorporation of Ni and Cu into Nb$_2$O$_5$ reduced the band gap energy from 3.3 to 2.8 eV, enabling efficient utilization of visible light. Moreover, NiCu/Nb$_2$O$_5$ exhibited the highest E2 removal efficiency (82%) under UV-A-assisted conditions at a concentration of 1.5 g L^{-1}. The reaction kinetics were found to follow a second-order model with a rate constant of $k = 0.0020$ L g^{-1} min^{-1}, and a plausible reaction mechanism was proposed. Through the study of radical elimination, it was proven that the radical oxidation reaction mechanism predominated in the reaction. The results of the toxicity assays, combined with the TOC parameter, demonstrated the efficacy of photocatalytic degradation in reducing E2. These findings demonstrate the great potential of the NiCu/Nb$_2$O$_5$ photocatalyst for removing persistent pollutants.

Introduction

The contamination of aquatic matrices by emerging pollutants is a critical and urgent issue, given the ability of these compounds to persist in the environment and their potential for negative impacts on ecosystems (Parida et al. 2021; Majumder and Gupta 2021; Nippes et al. 2022b). Furthermore, among the emerging pollutants, there are compounds known as endocrine disruptors (EDs), a class of substances capable of significantly impacting human health, increasing the risk of cancer, and causing disorders in the immune and nervous systems, even at low concentrations (Segner 2006; Orozco-Hernández et al. 2019).

Among the EDs, estrogenic steroids are highly dangerous, given the adverse effects they can cause in environmental ecosystems (Du et al. 2020). 17β-Estradiol (E2) is particularly concerning, as it is recognized as the most potent estrogen and has been widely detected in various aquatic matrices (Yu et al. 2019). E2 is a natural estrogen primarily used in hormone replacement therapy and birth control (Omar et al. 2016) and is primarily introduced into environmental waters through animal and human urine (Kabir et al. 2015; Orozco-Hernández et al. 2019). Some effects of this estrogen have been reported in the literature, such as increased cancer risk and deformities in humans, reproductive organ modifications, and sex alteration in fish (Purdom et al. 1994; Qing et al. 2022). The difficulty of conventional treatment processes in removing compounds like E2 highlights the need for alternative water treatment technologies that can complement traditional methods and eliminate this threat from effluents (Majumder and Gupta 2020).

In this context, we highlight the process of heterogeneous photocatalysis, a promising and environmentally friendly water treatment technology, due to its ease of use and ability to mineralize various water contaminants

---

Responsible Editor: Sami Rtimi

✉ Ramiro Picoli Nippes
  ramiro_picoli@yahoo.com.br

1 Chemical Engineering Department of Maringa State University, Maringa, PR, Av. Colombo Zone 7, Brazil 579087020-900

into non-hazardous compounds (Yin et al. 2010; Arora et al. 2022). This process employs semiconductors (such as $BiVO_4$, CeO_2, Fe_2O_3, MnO_2, TiO_2, ZnO, and Nb_2O_5) as fine solids or nanostructures (Boughelout et al. 2020). Nb_2O_5 is one of these semiconductors, which is a transition metal oxide of the n-type with a band gap energy value (Eg) of approximately 3.0–3.4 eV, making it an attractive candidate for photocatalysis (Su et al. 2021). Due to its good chemical stability, non-toxicity, and commercial availability (Yan et al. 2014), Nb_2O_5 finds extensive use in photocatalysis (Hu and Liu 2015; Souza et al. 2016; Goswami et al. 2022; Ücker et al. 2022a, 2023a, b; Yang et al. 2022; Lenzi et al. 2022; de Almeida et al. 2022; Liu et al. 2023). Additionally, Brazil is one of the main producers of niobium, making Nb2O5 a valuable material for use in water treatment applications (Nowak and Ziolek 1999).

Given the potential for photocatalytic application, Nb_2O_5 can still have its photocatalytic activity enhanced through the use of modification techniques such as functionalization (Lin et al. 2011; Furukawa et al. 2012; Peng et al. 2021; Xia et al. 2022), heterojunctions (Yan et al. 2014; da Silva et al. 2017; Sacco et al. 2020), and addition of transition metals (such as Ag, Fe, Cu, Ni, Pt, Au, etc.) (Vivek et al. 2022). Additionally, recently, it has been discovered that bimetallic nanostructures in semiconductors are effective in various catalytic processes, due to the synergistic effect of combining two metals (Riaz et al. 2020; Vivek et al. 2022; Nippes et al. 2022a). In particular, bimetallic copper and nickel catalysts have been reported as an efficient method to increase reaction efficiency, including in heterogeneous photocatalysis (Riaz et al. 2020). However, further studies are needed to understand the effects of this methodology and its application in the development of Ni and Cu bimetallic catalysts incorporated into Nb_2O_5 that are efficient in removing EDs such as E2. It is important to note that we did not find any literature reports on the photocatalytic degradation of the 17β-estradiol molecule using Nb_2O_5, either in its pure form or functionalized form.

Therefore, the objective of this study was to evaluate the degradation of the estrogen E2 using the semiconductor Nb_2O_5 in its raw form and also to explore the design of a bimetallic copper and nickel (Cu: Ni) catalyst supported on Nb_2O_5, establishing a relationship between the physicochemical properties of this new photocatalyst and its photocatalytic performance in the degradation of E2 in an aqueous medium, in a UV-A irradiation-assisted photocatalytic system. The efficiency of the photocatalytic process was also evaluated in terms of effluent toxicity, using two bioindicators (*Artemia salina* and *Lactuca sativa*), which provide highly relevant results from a toxicological perspective.

Materials and methods

Materials

For the synthesis of the material, nickel nitrate ($Ni(NO_3)_2 \cdot 6H_2O$, 97%) and copper nitrate ($Cu(NO_3)_2 \cdot 3H_2O$, 98%), both obtained from Sigma-Aldrich, were used along with niobic acid (HY-340) provided by Brazilian Company of Metallurgy and Mining (BCMM). The HY-340 was calcined to obtain niobium (V) oxide (Nb_2O_5). For toxicity tests, sodium chloride (NaCl, 99%) and potassium dichromate ($K_2Cr_2O_7$, 99%) from Synth were used. *Lactuca sativa* seeds and *Artemia salina* cysts were obtained from an agricultural supplier. For scavengers tests, the reagents ethylenediaminetetraacetic acid (EDTA, 99%), isopropanol (($CH_3)_2CHOH$, 99.9%), and potassium iodide (KI, 99%), all obtained from Sigma-Aldrich, were used. Laboratory-grade water (LGW, 18 MΩ) was prepared using a Millipore purification system. The synthetic hormone 17β-estradiol (> 98%) was obtained from Sigma-Aldrich, and Table 1 present its main characteristics.
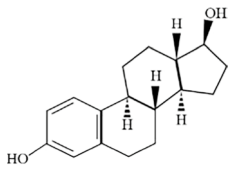
Methods

Synthesis

The catalyst used in this study was $NiCu/Nb_2O_5$ containing 1% Cu and 5% Ni by mass, which were determined by preliminary tests. The catalyst was prepared through a wet impregnation method by adding copper and nickel nitrates to niobium pentoxide. The resulting precursor was dried at 100 °C for 24 h and then calcined at 500 °C for 4 h, yielding a brown solid material.

Characterization

The catalysts were characterized by textural analysis using nitrogen gas (N_2) physisorption studies (Quantachrome, model NOVA-1200). The morphology of the materials was observed by scanning electron microscopy (SEM) (Shimadzu SS-550 software, Superscan SS-550), atomic force microscopy (AFM) conducted on an atomic force microscope (Shimadzu SPM-9700) in the threading mode using a Silicon-Pt/Ir coated tip (spring constant of 0.5–9.5 N/m and at a frequency of 45–115 Hz), and transmission electron microscopy (TEM) using a JEOL transmission electron microscope, model JEM-1400. X-ray fluorescence spectroscopy (XRF) was performed on a Rigaku ZSX Primus II equipment using oxide standards. Atomic

Table 1 Properties of 17β-estradiol (E2)

Molecular formula	$C_{18}H_{24}O_2$
CAS number	50-28-2
Molecular Weight	272.39 g mol^{-1}
Chemical Structure	
Ionization constant (pKa)	10.4
Solubility	13 mg L^{-1} (20°C)
λ max	280 nm

absorption (AA) was performed on a Thermo Scientific iCE3000 to determine the metal composition.

The structural properties of the catalysts were analyzed by an X-ray diffractometer Shimadzu (model XRD-6000, 2Θ range 2 to 95°, CoKα radiation, with speed 2°/min, voltage 40 kV, and current 50 mA) and Fourier transform infrared spectroscopy (FTIR) on a Bruker Spectrometer (model Vertex 70 v, resolution 4 cm^{-1}, 128 scans, spectral range 4000–400 cm^{-1}).

The optical properties of the photocatalysts were examined using photoacoustic spectroscopy, performed on a spectroscopy module operated with 21 Hz frequency modulation in the range 200 to 800 nm, and normalized with ultra-pure carbon spectrum. The band gap energy was calculated using Tauc's direct method. Photoluminescence spectrometer was performed on a PerkinElmer luminescence spectrometer, LS-50B, in the spectral region of 350 to 600 nm.

Reactional tests

The reaction system used in the experiments was isolated from the external environment by an aluminum metal box, equipped with two side fans for cooling (Fig. 1). The system consists of a batch-operated beaker equipped with a magnetic stirrer and five UV-A tubular lamps. The lamps measure 26 mm × 450 mm with a power of 45 W, providing a light intensity of 0.064 W m^{-2}. Each test used an initial concentration (C_0) of 10 mg L^{-1} of E2 in 250 mL of solution, with the photocatalyst mass ranging from 1 to 2 g L^{-1}. The reactions were carried out at room temperature and at the natural pH of the solution. Samples were collected at specific time intervals (0, 15, 30, 60, 90, 120, 150, and 180 min) using a plastic syringe connected to a hose and passed through 0.22-μm Millipore membranes supported by
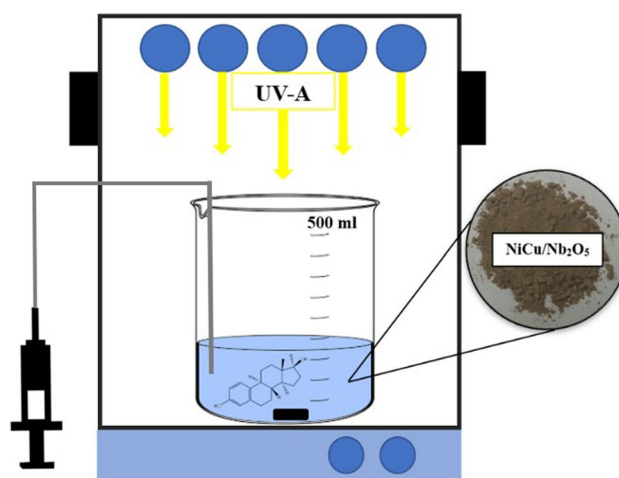

Fig. 1 Reaction module for photocatalytic tests with NiCu/Nb$_2$O$_5$ for E2 degradation in aqueous media

stainless steel. The efficiency of E2 removal by adsorption (absence of light) and by photolysis (absence of catalyst) was also evaluated. The main active species of the photocatalytic reaction and degradation process were investigated by adding radical scavengers such as 1 mM EDTA (h$^+$ scavenger), 10 mM isopropanol (HO$^.$ scavenger), and 10 mM potassium iodide (HO$^.$ and h$^+$ scavenger) during the photocatalytic reaction experiments (Upreti et al. 2016). The residual E2 concentration in the treated solutions was quantified via HPLC (Shimadzu HPLC, 10A VP) using a C18 column (250 × 4.6 mm, 5 μm, Hichrom) (Isecke et al. 2018). An isocratic mobile phase composed of a mixture of acetonitrile/water 80: 20 (v/v) at a flow rate of 1.0 mL min^{-1} was used. The UV detector was set at 210 and 280 nm. Prior to the analysis, a calibration curve was generated using E2

solutions with known concentrations (1–15 mg L^{-1}). The retention time for E2 was approximately 3.75 min. Analysis of the treated effluent generated after treatment included quantification of total organic carbon (TOC) following the methodology described in standard methods (APHA 1999). TOC was determined using a Shimadzu TOCL analyzer, and all analyses were performed in triplicate.

Kinetics study

To choose the best model that describes the best result obtained by this study, a mathematical method was proposed in which the reaction order was varied: zero order, ½ order, first order, and second order, according to Eq. 1, where *n* is the respective reaction order. The fitting of the models to the experimental data was performed by the numerical method in MATLAB® software, starting from the differential equation below. The differential equation was solved using the 4th-order Runge–Kutta.

$$\frac{dC_A}{dt} = -kC_A^n \tag{1}$$

Catalyst reuse

The NiCu/Nb$_2$O$_5$ photocatalyst was evaluated for its regeneration and subsequent reuse in new E2 degradation cycles. After each execution, the photocatalyst was removed from the reaction vessel by filtration and then washed thoroughly with deionized water and finally dried in an 80 °C oven overnight. Atomic absorption (AA) was performed on a Thermo Scientific iCE3000 to evaluate the metal lixiviation.

Toxicity test

Toxicity tests were conducted to determine the optimal degradation condition using *Artemia salina* and *Lactuca sativa* (lettuce), a species of microcrustacean and plant, respectively. These bioindicators possess fundamental characteristics to respond to environmental changes, even at low levels of contaminant concentration (Silveira et al. 2017).

The methodologies employed were based on the germination of *Lactuca sativa* seeds to calculate the relative germination rate (RGR) and the relative root length rate (RLR) and on the hatching of *Artemia salina* cysts to determine the lethal concentration (LC$_{50}$) after exposure to the treated effluent. Guidelines for these methodologies can be found in the work of Nippes et al. (2021b).

Results and discussion

NiCu/Nb$_2$O$_5$ characterization

Figure 2a shows the diffractograms of both the Nb$_2$O$_5$ support and the NiCu/Nb$_2$O$_5$ catalyst. The diffractogram of Nb$_2$O$_5$ (PDF #27–1003) indicated an orthorhombic crystal structure. Wet impregnation did not alter the structure of the support, as the same Nb$_2$O$_5$ peaks were observed in the matrix. However, incorporation of the metals led to the formation of dispersed oxides on the surface. The catalyst displayed diffraction peaks for NiO (PDF #73–1523) which exhibited a cubic crystalline structure at 43.1° and 62.8°. Copper diffraction peaks were not detected due to its low content in the catalyst, as previously reported in the literature (Dancini-Pontes et al. 2015; Da Silva et al. 2016). Nonetheless, the presence of copper can be identified in the
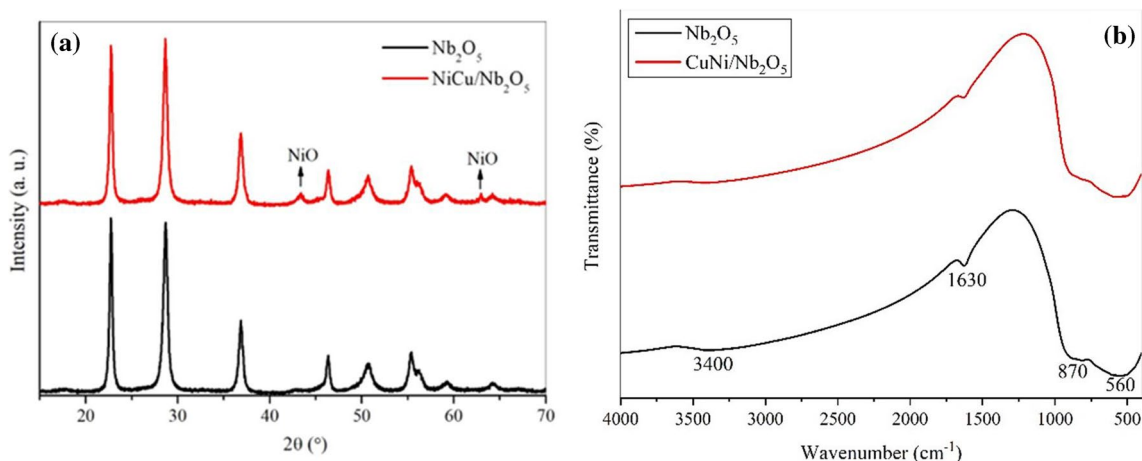

Fig. 2 Diffractograms (**a**) and infrared spectroscopy profiles (**b**) of the Nb$_2$O$_5$ and NiCu/Nb$_2$O$_5$ samples

X-ray fluorescence and atomic absorption analyses presented in Table 2, which show the chemical composition of the samples.

Figure 2b shows the Fourier transform infrared spectroscopy (FTIR) analysis profiles of the support and catalyst. The samples showed very similar spectra, both in frequency and intensity. Both analyses point out bands around 560 cm^{-1} and 870 cm^{-1} characteristics of Nb_2O_5 of orthorhombic structure (Graça et al. 2013; Ramanjaneya Reddy and Chennakesavulu 2014), as observed in the X-ray diffractograms.

The support and the catalyst showed bands around 1630 cm^{-1} and 3400 cm^{-1}, characteristic of the OH functional group (De Oliveira-Cantão et al. 2010), being the intensity of the bands in the catalyst lower, indicating the elimination of part of the OH functional groups from the surface by the incorporation of copper and nickel.

Textural analysis results were obtained from N_2 adsorption/desorption isotherms and are presented in Table 3 and Fig. 3. Comparing the support and the catalyst, it can be seen that impregnation results in a decrease in the specific area compared to that of the support, possibly due to the accommodation of oxides in internal regions to the pores, which justifies the reduction of pore volume (Furtado et al. 2011; Da Silva et al. 2016; Chan et al. 2017). Despite this, both remained as mesoporous material.

It is observed in the isotherms that the impregnation of the copper and nickel oxides did not significantly alter the adsorption isotherms. The isotherms are of type IV, and the hysteresis is of type H2, indicating that the pore shapes are poorly defined (Steele 1983).

Considering the proportion of nickel and copper in the oxides observed in the XRF analysis, the mass content of nickel is 4.87%, and copper is 0.95%, close to the values obtained by atomic absorption. Thus, the results show that the impregnation of the metals of the active phase to the supports was quite satisfactory, considering the proximity between the theoretical and real values.

The morphology of the materials was observed through scanning electron microscopy (SEM) and atomic force

Table 2 Chemical composition of catalysts by XRF and AA techniques

FRX			AA	
Samples	Component	Mass content (%)	Component	Mass content (%)
Support	Nb_2O_5	99.99	-	-
Catalysts	Nb_2O_5	92.61	-	-
	NiO	6.20	Ni	4.90
	CuO	1.19	Cu	0.95

Table 3 Textural analysis by N_2 adsorption/desorption

Sample	Specific area BET (m^2 g^{-1})	Pore volume (cm^3 g^{-1})	Average pore radius (Å)
Nb_2O_5	77.2	0.167	45.5
NiCu/Nb_2O_5	44.7	0.146	24.1

microscopy (AFM), and the result is presented in Fig. 4a and b. Both images showed a heterogeneous surface formed by irregular particles, with some agglomerates but similar structures. This same configuration is observed in the MFA images for the samples, with a similar tendency for agglomeration of the particles. The result confirms that the incorporation of the metals did not result in significant changes in the morphology of Nb_2O_5.

Figure 4c and d show the TEM images and particle distribution of Nb_2O_5 and NiCu/Nb_2O_5. Both samples showed similar morphology, confirming no changes in the support structure occurred after impregnation. A clustering of round-shaped particles with different contrasts is also observed in the catalyst sample. The particles observed in the support range of 10 to 70 nm with an average size of 40 nm, while the catalyst is in size range of 10 to 60 nm with an average size of 31 nm. This reduction in average particle size suggests that incorporating the metals may suppress the aggregation of the Nb_2O_5 particles. This effect may provide greater availability of the active sites for OH radical generation and enhance the photocatalysis process.

Figure 5a shows the direct Tauc plotting method for the photoacoustic spectra of the Nb_2O_5 and NiCu/Nb_2O_5 photocatalysts, along with the obtained band gap values for each catalyst in eV. The value found for the pure Nb_2O_5 was 3.3 eV, a value consistent with what is expected for
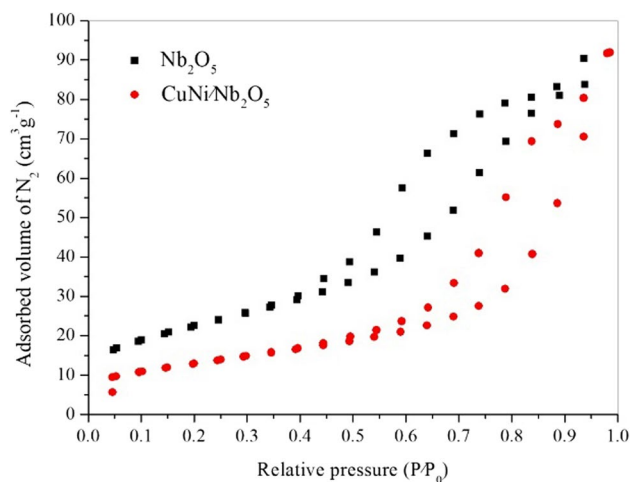

Fig. 3 N_2 adsorption/desorption isotherms of the samples
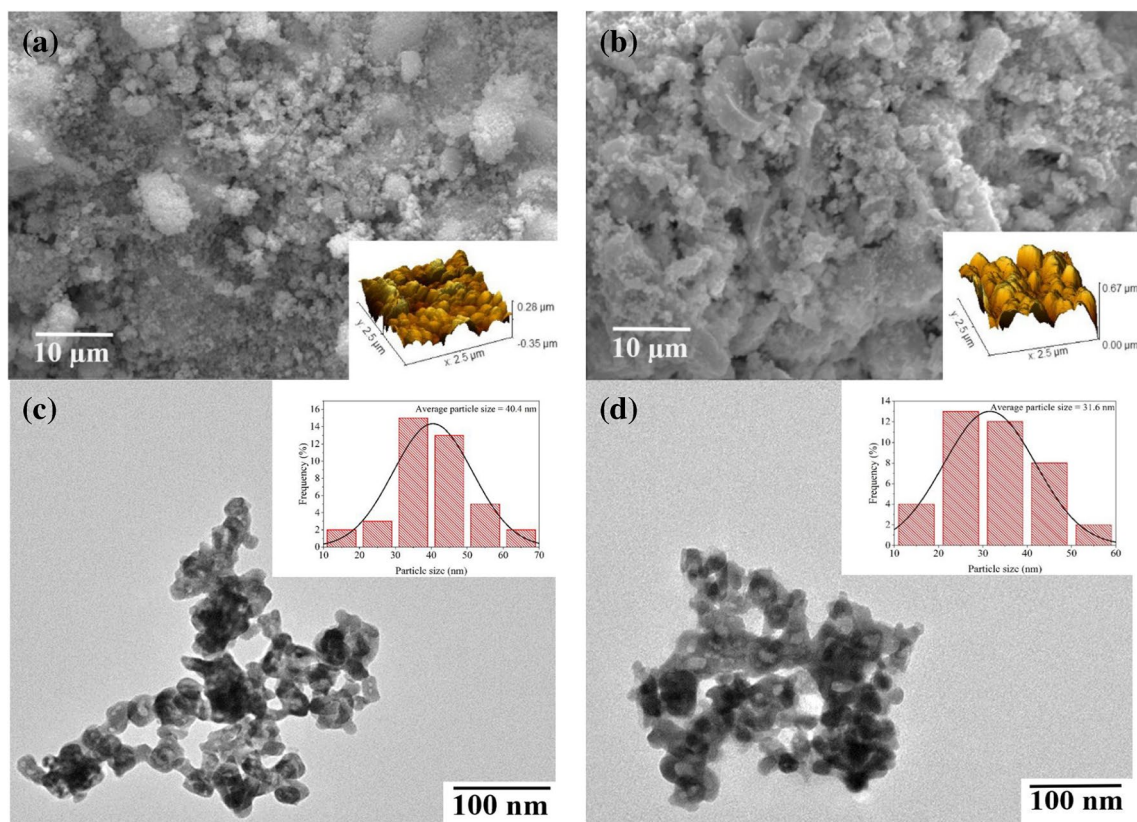
Fig. 4 SEM at ×10,000 magnification and MFA of (**a**) Nb_2O_5 and (**b**) $NiCu/Nb_2O_5$ and MET of (**c**) Nb_2O_5 and (**d**) $NiCu/Nb_2O_5$ and respective particle size distributions

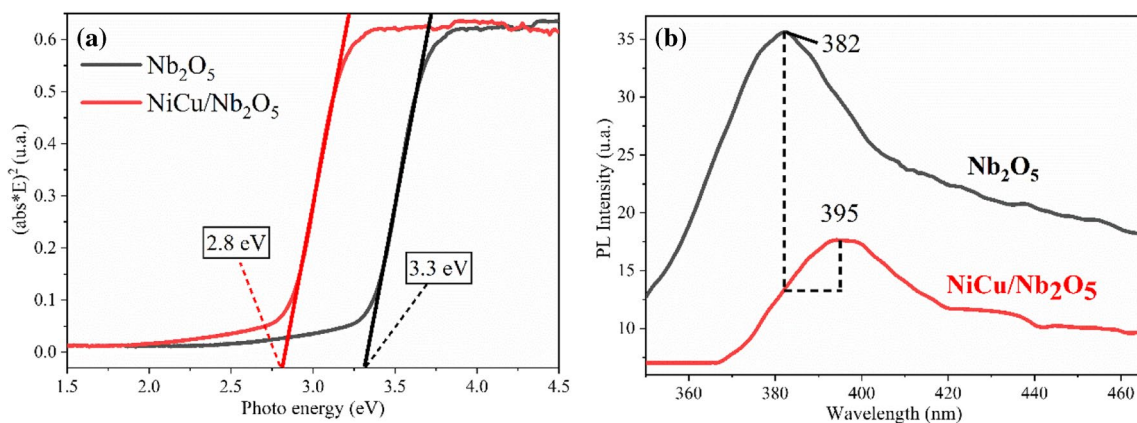**Fig. 5** Photoacoustic (**a**) and photoluminescence (**b**) spectra of Nb_2O_5 and $NiCu/Nb_2O_5$ photocatalysts

this material (Silva et al. 2020). However, the band gap value was reduced to 2.8 eV for the modified photocatalyst, extending its photon absorption spectrum to the visible region (> 400 nm). This effect results from the addition of nickel and copper, which can improve the absorption ability of optical radiation and reduce the photocatalyst gap due to the synergistic effect of combining the two metals (Jin and Zhang 2020; Vivek et al. 2022).

The presence of the metals also caused optical changes in the material, as can be observed in the photoluminescence (PL) spectrum, shown in Fig. 5b. For the pure Nb_2O_5, it was visualized that a more robust and intense emission peak present in the UV region at 382 nm is due to the emission peak of Nb_2O_5. On the other hand, for the bimetallic material, it was noticed that a reduction in the intensity of the spectrum indicates that the addition of Ni and Cu inhibits the charge
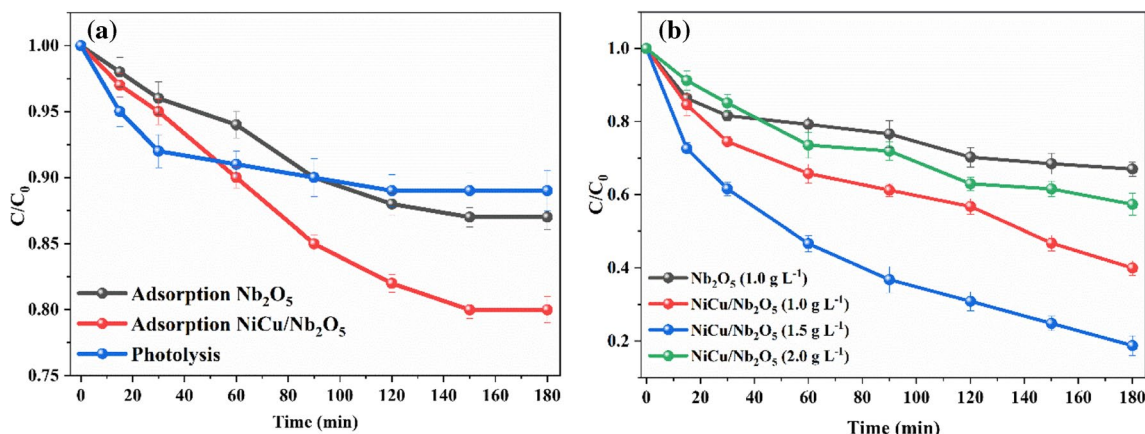
Fig. 6 Results of the E2 hormone removal tests in aqueous media through adsorption, photolysis (**a**), and photocatalysis (**b**)

recombination process, which favors the performance of the photocatalyst, improving the photocatalysis process (Nippes et al. 2021a; Ücker et al. 2022b). Furthermore, a shift of the main emission peak to the more extended wavelength region was also detected, reinforcing the possible activation of the photocatalyst in the near visible region.

Reactional tests

Figure 6 shows the results obtained for the photocatalytic tests. To begin with, it is essential to evaluate the contribution of the photolysis and adsorption processes in removing E2. In percentage, photolysis was responsible for 9% of E2 removal, while adsorption reached values close to 14 and 20% for Nb_2O_5 and $NiCu/Nb_2O_5$, respectively. The result confirms that the addition of catalyst plus radiation is necessary to degrade the E2 hormone effectively.

With the catalysts activated with UV-A radiation, it was observed that pure Nb_2O_5 could remove approximately 33% of E2. On the other hand, the catalyst modified with Ni and Cu at the same mass concentration reached 43% degradation. This proves that the functionalization of Nb_2O_5 with the metals efficiently improved the photocatalytic activity, evidenced by the reduction of its band gap energy, which allowed its activation at wavelengths in the UV-A region.

Comparing the catalyst loadings employed (g L^{-1}), it is evident that the increase from 1.0 to 1.5 g L^{-1} causes an increase in E2 degradation (82%) due to the greater availability of active sites for the photocatalytic reaction. However, the increase to 2.0 g L^{-1} reduces the catalytic activity. This indicates interference in the amount of catalyst applied due to the excess turbidity of many particles in the aqueous medium. This hinders the insertion of radiation into the system. With the result, we conclude that 1.5 g L^{-1} is the most appropriate concentration for the system.

Table 4 Kinetic fitting results using numerical interaction method

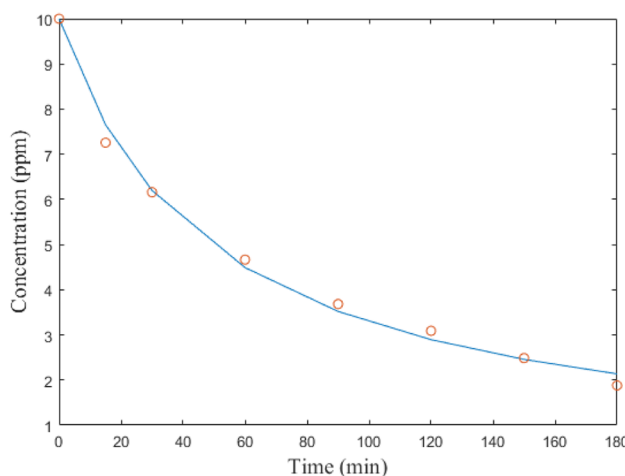| Reaction	k (L g^{-1} min^{-1})	R^2
Nb_2O_5 (1.0 g L^{-1})	0.00034	0.84
$NiCu/Nb_2O_5$ (1.0 g L^{-1})	0.00077	0.96
$NiCu/Nb_2O_5$ (1.5 g L^{-1})	0.00200	0.99
$NiCu/Nb_2O_5$ (2.0 g L^{-1})	0.00046	0.97

Fig. 7 Kinetic fit for second-order model of the $NiCu/Nb_2O_5$ reaction test

The behavior observed in the photocatalytic reaction was proven mathematically by the kinetic study. The values of the speed constant (k) and the fit (R^2) are presented in Table 4. The model that best fitted the data was the second-order model ($n = 2$). This indicates that the initial speed of micropollutant consumption is higher in the first minutes of the reaction (Fig. 7). Over time, the changes in compound concentration are less significant, indicating some resistance,

either in the production of hydroxyl radicals or in the access of E2 to these radicals. The highest value for k is for the reaction with the NiCu/Nb$_2$O$_5$ catalyst at a concentration of 1.5 g L^{-1}.
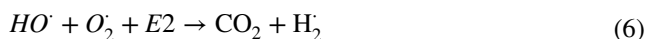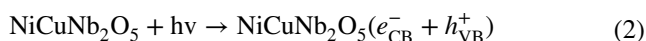
Experiments with radical scavengers were conducted to identify the main active species in the photocatalytic reaction and degradation process of the E2 contaminant. The EDTA was used as an h$^+$ scavenger, isopropanol as an $HO^.$ scavenger, and potassium iodide (KI) as a scavenger for both $HO^.$ and h$^+$ (Fig. 8). The addition of scavengers followed the order of potassium iodide > isopropanol > EDTA > no scavenger, over a 180-min reaction with [NiCu/Nb$_2$O$_5$] = 1.5 g L^{-1} and [E2] = 10 mg L^{-1}. The iodide ion is a scavenger that reacts with both positive holes (h$^+$) and surface hydroxyl radicals ($HO^.$) (Martin et al. 1995), whereas isopropanol is known to eliminate only surface hydroxyl radicals ($HO^.$) (Van Doorslaer et al. 2012). Both scavengers reduce the number of available oxidizing species on the catalyst's surface, thereby decreasing the degradation kinetics of E2. The addition of EDTA, which acts as an h$^+$ scavenger (Upreti et al. 2016), showed the least effect on the E2 photodegradation rate, suggesting that surface hydroxyl radicals ($HO^.$) act as the main oxidizing agents in this photocatalytic process, and the radical oxidation reaction mechanism predominates.

Reaction mechanism

Based on the results obtained in this study and the conducted literature review, the pure Nb$_2$O$_5$ semiconductor is activated under ultraviolet light (Silva et al. 2020). By introducing dopant ions into Nb$_2$O$_5$, the optical properties are improved by reducing the band gap value and shifting the semiconductor's activation to the visible region. This optical enhancement of the semiconductor ensures a longer lifetime for electron–hole pairs, providing greater opportunities for charge carriers to reach the catalyst surface and interact with dissolved organic compounds (Vasu et al. 2022). Additionally, the incorporation of Cu^{2+} and Ni^{2+} ions into the Nb$_2$O$_5$ network generates an oxygen defect that acts as an energy site for dissociating organic pollutants on the catalyst surface.

Thus, when visible light is irradiated on the NiCu/Nb$_2$O$_5$ catalyst, electrons are excited to the conduction band, leaving a hole in the valence band (Eq. 2). These holes in the valence band form hydroxyl radicals through the decomposition of water or by reacting with OH$^-$ (Eqs. 3 and 4). The electrons transferred to the surface of the conduction band react with dissolved oxygen, forming $O_2^{.-}$ ions (Eq. 5) which further react with water to produce $HO^.$ radicals. Ultimately, both $HO^.$ and $O_2^{.-}$ ions promote the mineralization of the E2 molecule (Eq. 6), transforming the pollutant into CO$_2$ and H$_2$O. Figure 9 depicts the suggested possible mechanism for the degradation of E2 molecules.

$$NiCuNb_2O_5 + h\nu \rightarrow NiCuNb_2O_5(e_{CB}^- + h_{VB}^+) \tag{2}$$

$$h_{VB}^+ + H_2O \rightarrow H^+ + HO^. \tag{3}$$

$$h_{VB}^+ + OH^- \rightarrow HO^. \tag{4}$$

$$e_{CB}^- + O_2 \rightarrow O_2^{.-} \tag{5}$$

$$HO^. + O_2^. + E2 \rightarrow CO_2 + H_2 \tag{6}$$

where h^+ is the photogenerated hole, e^- is the photogenerated electron, VB is the valence band, and CB is the conduction band.

In most cases, the oxidation of organic pollutants using a combination of semiconductors and light involves the generation of the hydroxyl radical, which exhibits high oxidation potential (2.80 eV). Generally, the hydroxyl radical can oxidize organic compounds through three mechanisms: electron transfer, hydrogen abstraction, and electrophilic addition (Legrini et al. 1993). Although this article does not present the degradation pathways of the pollutant, the total organic carbon (TOC) parameter indicated that the E2 molecule degraded, forming possible inorganic substances such as CO$_2$ and H$_2$O, resulting in approximately 81% reduction in organic carbon during the pollutant degradation process.

Table 5 presents the results obtained by other studies on the degradation of the hormone 17β-estradiol. The results obtained in this work are similar to those of other studies; however, in some cases, the performance of the photocatalyst is inferior. Nevertheless, it is worth noting that, besides achieving a photocatalytic degradation of E2 higher than
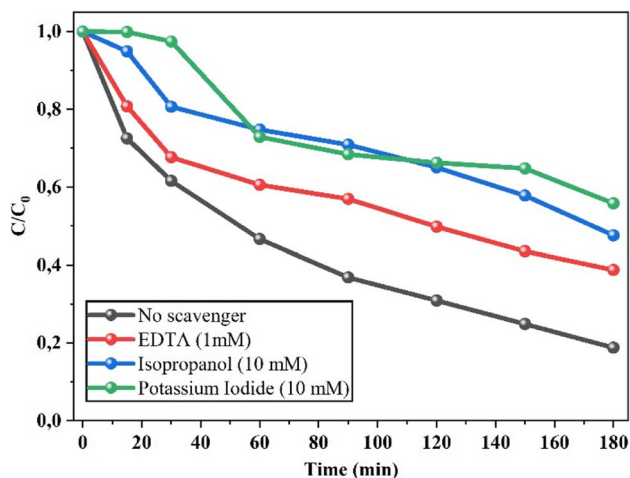

Fig. 8 Photocatalytic degradation experiments in the presence of various scavengers

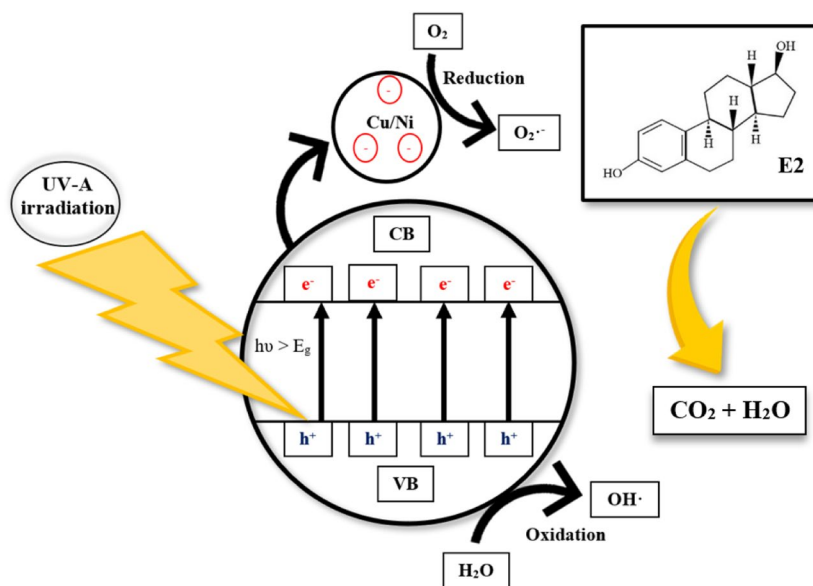**Fig. 9** Possible electron transfer reaction mechanism

Table 5 Catalytic degradation of E2 with different nanoparticles

Catalyst	Experimental conditions	Efficiency (%)	TOC removal (%)	Ref
NiCu/Nb$_2$O$_5$ (1.5 g/L)	UV-A; natural pH	82	81	This work
Pth-Al-ZnO (40 mg/ml)	UV-A; pH 6.5	96	90	Majumder and Gupta (2020)
MnO$_2$/TNTs (0.1 g/L)	Simulated sunlight; pH 5	99	82.6	Du et al. (2018)
ZnO nanorod arrays (1.85 µM)	UV-A and blue lights	80	-	Liu and Gao (2014)
Ag/TiO$_2$ film	28W black-light; pH 6.5	97	-	Lima et al. (2019)

80%, our study observed a significant removal of TOC, strongly indicating compound mineralization. Additionally, the reduction of E2 toxicity in water, as presented below, represents a significant advancement for the application of the photocatalysis process using NiCu/Nb$_2$O$_5$. The next steps involve studying the reaction variables and proposing an optimization to completely degrade E2 with a significant reaction kinetics.

Catalyst reuse

At this stage, we investigated the stability of our photocatalyst and its application in consecutive reaction cycles. This is a highly relevant step to verify the stability and recyclability of the produced material, as well as a crucial parameter for the techno-economic feasibility of the process. In this case, the NiCu/Nb$_2$O$_5$ sample was used for seven consecutive reaction cycles in the removal of the hormone E2 from an aqueous solution, with the results presented in Fig. 10. The results showed that the photocatalytic material exhibited good stability, maintaining a removal percentage of approximately 70%. Additionally, the resulting solution after the reaction was analyzed using atomic absorption technique, and no presence of
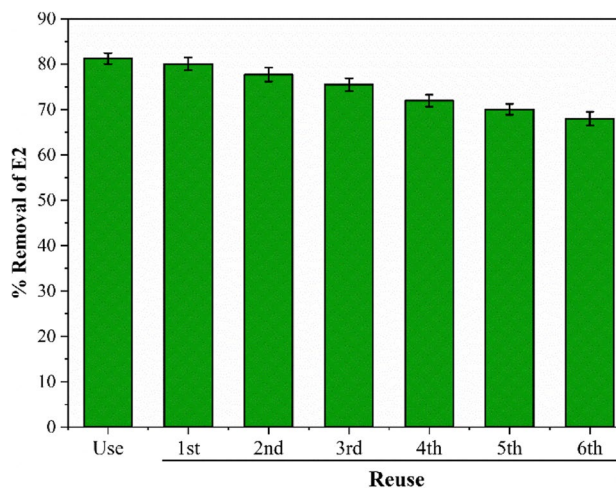

Fig. 10 Recycling tests for the photocatalytic capacity of NiCu/Nb$_2$O$_5$

the metals incorporated into Nb$_2$O$_5$ was detected. This confirms that the impregnation technique was efficient in fixing the metallic species onto the semiconductor, and the photocatalyst will not cause pollution of the solution with nickel or copper, thus can be safely applied in an aqueous medium.

Table 6 Toxicity assessment against *Lactuca sativa*

Samples	Germinated seed	Mean root length (cm)	Relative seed germination (%)	Relative root length (%)
Negative control	0	0	0	0
Positive control	10	2.36 ± 0.20	100	100
Initial effluent	7	1.33 ± 0.15	70	56
Treated effluent	9	2.14 ± 0.25	90	91

Table 7 Toxicity assessment against *Artemia salina*

Samples	LC_{50}	Concentration (mg L^{-1})	Mortality (%)
Control	1.45	28.18	100
Effluent non-treated	2.15	141.25	57
Effluent treated	-	> 200.00	3

Toxicity test

The photocatalytic degradation process can generate sub-products with concerning toxicity, which must be taken into consideration to ensure its effective application. In order to evaluate the toxicity of the resulting effluent, we used two bioindicators, *Lactuca sativa* and *Artemia salina*.

Tests with *Lactuca sativa* were conducted in triplicate using negative control, positive control, untreated synthetic effluent samples, and synthetic effluent samples after treatment. The results presented in Table 6 indicate that 100% relative germination was achieved for the treated samples, while for the untreated sample, it was 60%. In terms of relative root growth, it was 91% for the treated sample and 70% for the untreated sample, demonstrating that the application of the photocatalytic process using NiCu/Nb$_2$O$_5$ as a catalyst was effective in reducing the toxicity of the effluent.

The *Artemia salina* tests treatment. This is because the LC$_{50}$ parameter (Table 7), which corresponds also confirmed that the toxicity of the solution containing the hormone E2 was reduced after to the median lethal concentration, showed a value greater than 200 mg L^{-1} and a mortality rate of 3%. Thus, it is possible to assert that the final effluent was non-toxic after the photocatalytic treatment. These results are of utmost importance because, as reported in the literature, the estrogen E2 has negative effects on aquatic organisms even at low concentrations (Ahmad et al. 2009; Orozco-Hernández et al. 2019). Therefore, the development of effective technologies to reduce the danger of this type of compound in water is of fundamental importance.

Conclusion

The NiCu/Nb$_2$O$_5$ photocatalyst was synthesized via the wet impregnation method and exhibited irregular shapes with a surface area of 44.7 m^2 g^{-1}. The synthesis effectively incorporated the metals into the niobium surface, as confirmed by atomic absorption and FRX techniques, without altering the structure of the support. The diffractograms of the Nb$_2$O$_5$ support and the NiCu/Nb$_2$O$_5$ catalyst revealed the same orthorhombic crystal structure of Nb$_2$O$_5$, with the incorporation of dispersed oxides on the surface. The catalyst showed a higher rate of E2 degradation than the crude Nb$_2$O$_5$ under the same reaction conditions, with a maximum photocatalytic degradation of 82% for 10 mg L^{-1} E2 at a catalyst loading of 1.5 g. Incorporating Ni and Cu into Nb$_2$O$_5$ led to an improvement in its photocatalytic performance and activation at wavelengths in the visible region (< 400 nm). The degradation reaction of E2 followed a second-order model. Toxicity tests have demonstrated a substantial decrease in the negative effects associated with E2. The TOC result corroborates these findings, providing evidence for the effectiveness of the NiCu/Nb$_2$O$_5$ catalyst in achieving this outcome. Finally, the results obtained in this study are crucial for future application of this photocatalytic system on a large scale, such as in municipal wastewater treatment plants.

Declarations

Ethics approval Not applicable.

Consent to participate All authors participate to this work.

Consent for publication All authors accept to publish this work.

Competing interests The authors declare no competing interests.

References

Ahmad I, Maria VL, Pacheco M, Santos MA (2009) Juvenile sea bass (Dicentrarchus labrax L.) enzymatic and non-enzymatic antioxidant responses following 17β-estradiol exposure. Ecotoxicology 18:974–982. https://doi.org/10.1007/s10646-009-0369-3

APHA (1999) Standard methods for the examination of water and wastewater APHA, AWWA, and WEF, 20th edn. Washington, DC

Arora I, Chawla H, Chandra A et al (2022) Advances in the strategies for enhancing the photocatalytic activity of TiO_2: conversion from UV-light active to visible-light active photocatalyst. Inorg Chem Commun 143:109700. https://doi.org/10.1016/J.INOCHE.2022.109700

Boughelout A, Macaluso R, Kechouane M et al (2020) Photocatalysis of rhodamine B and methyl orange degradation under solar light on ZnO and Cu_2O thin films. React Kinet Mech Catal 129:1115–1130. https://doi.org/10.1007/s11144-020-01741-8

Chan X, Pu T, Chen X et al (2017) Effect of niobium oxide phase on the furfuryl alcohol dehydration. Catal Commun 97:65–69. https://doi.org/10.1016/J.CATCOM.2017.04.019

Da Silva FA, Pontes ID, Wurzler GT et al (2016) Production of hydrogen from bioethanol in Cu-Ni/$NbxOy$ catalysts obtained by different preparation methods. Int J Hydrogen Energy 41:8111–8119. https://doi.org/10.1016/j.ijhydene.2015.12.215

da Silva GTST, Carvalho KTG, Lopes OF, Ribeiro C (2017) g-C3N4/Nb_2O_5 heterostructures tailored by sonochemical synthesis: enhanced photocatalytic performance in oxidation of emerging pollutants driven by visible radiation. Appl Catal B 216:70–79. https://doi.org/10.1016/j.apcatb.2017.05.038

Dancini-Pontes I, DeSouza M, Silva FA et al (2015) Influence of the CeO_2 and Nb_2O_5 supports and the inert gas in ethanol steam reforming for H2 production. Chem Eng J 273:66–74. https://doi.org/10.1016/j.cej.2015.03.032

de Almeida AR, Casanova Monteiro F, Monteiro Frederico Haas Leandro, J, et al (2022) Photocatalytic oxidation of textile dye using sugarcane bagasse-Nb2O5 as a catalyst. J Photochem Photobiol A Chem 432:114103. https://doi.org/10.1016/j.jphotochem.2022.114103

De Oliveira-Cantão F, De Carvalho MW, Oliveira LCA et al (2010) Utilization of Sn/Nb_2O_5 composite for the removal of methylene blue. Quim Nova 33:528–531. https://doi.org/10.1590/s0100-40422010000300007

Du P, Chang J, Zhao H et al (2018) Sea-buckthorn-like MnO_2 decorated titanate nanotubes with oxidation property and photocatalytic activity for enhanced degradation of 17β-estradiol under solar light. ACS Appl Energy Mater 1:2123–2133. https://doi.org/10.1021/acsaem.8b00197

Du B, Fan G, Yu W et al (2020) Occurrence and risk assessment of steroid estrogens in environmental water samples: a five-year worldwide perspective. Environmental Pollution 267:115405. https://doi.org/10.1016/j.envpol.2020.115405

Furtado AC, Alonso CG, Cantão MP, Fernandes-Machado NRC (2011) Support influence on Ni–Cu catalysts behavior under ethanol oxidative reforming reaction. Int J Hydrogen Energy 36:9653–9662. https://doi.org/10.1016/J.IJHYDENE.2011.05.063

Furukawa S, Tsukio D, Shishido T et al (2012) Correlation between the oxidation state of copper and the photocatalytic activity of Cu/Nb_2O_5. J Phys Chem C 116:12181–12186. https://doi.org/10.1021/jp303625m

Goswami T, Kumar S, Bheemaraju A et al (2022) TiO_2 nanoparticles and Nb_2O_5 nanorods immobilized rGO for efficient visible-light photocatalysis and catalytic reduction. Catal Letters. https://doi.org/10.1007/s10562-022-04000-8

Graça MPF, Meireles A, Nico C, Valente MA (2013) Nb_2O_5 nanosize powders prepared by sol–gel – structure, morphology and dielectric properties. J Alloys Compd 553:177–182. https://doi.org/10.1016/J.JALLCOM.2012.11.128

Hu B, Liu Y (2015) Nitrogen-doped Nb_2O_5 nanobelt quasi-arrays for visible light photocatalysis. J Alloys Compd 635:1–4. https://doi.org/10.1016/j.jallcom.2015.02.109

Isecke BG, Oliveira Neto JR, Salazar VCR et al (2018) Study of ethinylestradiol degradation by photolysis and photocatalysis heterogeneous. Revista Virtual de Quimica 10:963–976. https://doi.org/10.21577/1984-6835.20180068

Jin Z, Zhang L (2020) Performance of Ni-Cu bimetallic co-catalyst g-C3N4 nanosheets for improving hydrogen evolution. J Mater Sci Technol 49:144–156. https://doi.org/10.1016/J.JMST.2020.02.025

Kabir ER, Rahman MS, Rahman I (2015) A review on endocrine disruptors and their possible impacts on human health. Environ Toxicol Pharmacol 40:241–258. https://doi.org/10.1016/J.ETAP.2015.06.009

Legrini O, Oliveros E, Braun AM (1993) Photochemical processes for water treatment. Chem Rev 93:671–698. https://doi.org/10.1021/cr00018a003

Lenzi GG, Abreu E, Fuziki MEK et al (2022) 17 α-Ethinylestradiol degradation in continuous process by photocatalysis using Ag/Nb_2O_5 immobilized in biopolymer as catalyst. Top Catal 65:1225–1234. https://doi.org/10.1007/s11244-022-01624-3

Lima KV, Emídio ES, Pupo Nogueira RF et al (2019) Application of a stable Ag/TiO_2 film in the simultaneous photodegradation of hormones. J Chem Technol Biotechnol 10:2656–2663. https://doi.org/10.1002/jctb.6258

Lin HY, Yang HC, Wang WL (2011) Synthesis of mesoporous Nb_2O_5 photocatalysts with Pt, Au, Cu and NiO cocatalyst for water splitting. Catal Today 174:106–113. https://doi.org/10.1016/j.cattod.2011.01.052

Liu Y, Gao W (2014) Photodegradation of endocrine disrupting chemicals by ZnO nanorod arrays. Mol Cryst Liq Cryst 603:194–201. https://doi.org/10.1080/15421406.2014.967605

Liu H, Li X, Ma L et al (2023) In-situ growth of g-C3N4 nanosheets on Nb_2O_5 nanofibers for enhanced performance in photocatalysis and lithium-sulfur battery. Colloids Surf A Physicochem Eng Asp 670:131572. https://doi.org/10.1016/j.colsurfa.2023.131572

Majumder A, Gupta AK (2020) Enhanced photocatalytic degradation of 17β-estradiol by polythiophene modified Al-doped ZnO: optimization of synthesis parameters using multivariate optimization techniques. J Environ Chem Eng 8:104463. https://doi.org/10.1016/J.JECE.2020.104463

Majumder A, Gupta AK (2021) Kinetic modeling of the photocatalytic degradation of 17-β estradiol using polythiophene modified Al-doped ZnO: influence of operating parameters, interfering ions, and estimation of the degradation pathways. J Environ Chem Eng 9:106496. https://doi.org/10.1016/j.jece.2021.106496

Martin ST, Lee AT, Hoffmann MR (1995) Chemical mechanism of inorganic oxidants in the TiO_2/UV process: increased rates of degradation of chlorinated hydrocarbons. Environ Sci Technol 29:2567–2573. https://doi.org/10.1021/es00010a017

Nippes RP, Macruz PD, Neves Olsen Scaliante MH (2021) Toxicity reduction of persistent pollutants through the photo-Fenton process and radiation/H_2O_2 using different sources of radiation and neutral pH. J Environ Manage 289:112500. https://doi.org/10.1016/j.jenvman.2021.112500

Nippes RP, Macruz PD, Gomes AD et al (2022a) Removal of reactive blue 250 dye from aqueous medium using Cu/Fe

catalyst supported on Nb_2O_5 through oxidation with H_2O_2. React Kinet Mech Catal 135:2697–2717. https://doi.org/10.1007/s11144-022-02279-7

Nippes RP, Macruz PD, Scaliante MHNO (2022b) Enhanced photocatalytic performance under visible light of TiO_2 through incorporation with transition metals for degradation of 17α-ethynylestradiol. Int J Environ Sci Technol. https://doi.org/10.1007/s13762-022-04361-y

Nippes RP, Frederichi D, Scaliante Olsen, e MHN (2021a) Enhanced photocatalytic performance under solar radiation of ZnO through hetero-junction with iron functionalized zeolite. J Photochem Photobiol A Chem 418:1–8. https://doi.org/10.1016/j.jphotochem.2021.113373

Nowak I, Ziolek M (1999) Niobium compounds: preparation, characterization, and application in heterogeneous catalysis. Chem Rev 99:3603–3624. https://doi.org/10.1021/cr9800208

Omar TFT, Ahmad A, Aris AZ, Yusoff FM (2016) Endocrine disrupting compounds (EDCs) in environmental matrices: review of analytical strategies for pharmaceuticals, estrogenic hormones, and alkylphenol compounds. TrAC - Trends in Anal Chem 85:241–259

Orozco-Hernández L, Gómez-Oliván LM, Elizalde-Velázquez A et al (2019) 17-β-Estradiol: significant reduction of its toxicity in water treated by photocatalysis. Sci Total Environ 669:955–963. https://doi.org/10.1016/j.scitotenv.2019.03.190

Parida VK, Saidulu D, Majumder A et al (2021) Emerging contaminants in wastewater: a critical review on occurrence, existing legislations, risk assessment, and sustainable treatment alternatives. J Environ Chem Eng 9:105966. https://doi.org/10.1016/j.jece.2021.105966

Peng C, Xie X, Xu W et al (2021) Engineering highly active Ag/Nb_2O_5@Nb2CTx (MXene) photocatalysts via steering charge kinetics strategy. Chem Eng J 421:1–15. https://doi.org/10.1016/j.cej.2021.128766

Purdom CE, Hardiman PA, Bye VVJ et al (1994) Estrogenic effects of effluents from sewage treatment works. Chem Ecol 8:275–285. https://doi.org/10.1080/02757549408038554

Qing Y, Li Y, Guo Z et al (2022) Photocatalytic Bi2WO6/pg-C3N4-embedded in polyamide microfiltration membrane with enhanced performance in synergistic adsorption-photocatalysis of 17β-estradiol from water. J Environ Chem Eng 10:108648. https://doi.org/10.1016/j.jece.2022.108648

Ramanjaneya Reddy G, Chennakesavulu K (2014) Synthesis and characterization of Nb_2O_5 supported Pd(II)@SBA15: catalytic activity towards oxidation of benzhydrol and Rhodamine-B. J Mol Struct 1075:406–412. https://doi.org/10.1016/j.molstruc.2014.06.090

Riaz N, Hassan M, Siddique M et al (2020) Photocatalytic degradation and kinetic modeling of azo dye using bimetallic photocatalysts: effect of synthesis and operational parameters. Environ Sci Pollut Res 27:2992–3006. https://doi.org/10.1007/s11356-019-06727-1

Sacco O, Murcia JJ, Lara AE et al (2020) Pt–TiO_2–Nb_2O_5 heterojunction as effective photocatalyst for the degradation of diclofenac and ketoprofen. Mater Sci Semicond Process 107:104839. https://doi.org/10.1016/j.mssp.2019.104839

Segner H (2006) Comment on "Lessons from endocrine disruption and their application to other issues concerning trace organics in the aquatic environment." Environ Sci Technol 40:1084–1085. https://doi.org/10.1021/es051791d

Silva RRM, Oliveira JA, Ruotolo LAM et al (2020) Unveiling the role of peroxo groups in Nb_2O_5 photocatalytic efficiency under visible light. Mater Lett 273:127915. https://doi.org/10.1016/j.matlet.2020.127915

Silveira GL, Lima MGF, dos Reis GB et al (2017) Toxic effects of environmental pollutants: comparative investigation using Allium cepa L. and Lactuca sativa L. Chemosphere 178:359–367. https://doi.org/10.1016/J.CHEMOSPHERE.2017.03.048

Souza RP, Freitas TKFS, Domingues FS et al (2016) Photocatalytic activity of TiO_2, ZnO and Nb_2O_5 applied to degradation of textile

wastewater. J Photochem Photobiol A Chem 329:9–17. https://doi.org/10.1016/j.jphotochem.2016.06.013

Steele WA (1983) Adsorption surface area and porosity. J Colloid Interface Sci 94:597–598. https://doi.org/10.1016/0021-9797(83)90305-3

Su K, Liu H, Gao Z et al (2021) Nb 2 O 5 -based photocatalysts. Advanced Science 8:2003156. https://doi.org/10.1002/advs.202003156

Ücker CL, Riemke F, Goetzke V et al (2022) Facile preparation of Nb_2O_5/TiO_2 heterostructures for photocatalytic application. Chem Physics Impact 4:100079. https://doi.org/10.1016/j.chphi.2022.100079

Ücker CL, Riemke F, Goetzke V et al (2022) Facile preparation of Nb_2O_5/TiO_2 heterostructures for photocatalytic application. Chem Physics Impact 4:100079. https://doi.org/10.1016/J.CHPHI.2022.100079

Ücker CL, Goetzke V, Riemke FC et al (2023) The photocatalytic performance of Fe inserted in Nb_2O_5 obtained by microwave-assisted hydrothermal synthesis: factorial design of experiments. J Photochem Photobiol A Chem 435:114294. https://doi.org/10.1016/j.jphotochem.2022.114294

Ücker CL, Rodrigues FSM, de Cantoneiro R et al (2023) The superior photocatalytic performance of loofah sponges impregnated with Nb_2O_5. J Photochem Photobiol A Chem 441:114694. https://doi.org/10.1016/j.jphotochem.2023.114694

Upreti AR, Li Y, Khadgi N et al (2016) Efficient visible light photocatalytic degradation of 17α-ethinyl estradiol by a multifunctional Ag–AgCl/ZnFe 2 O 4 magnetic nanocomposite. RSC Adv 6:32761–32769. https://doi.org/10.1039/C6RA00707D

Van Doorslaer X, Heynderickx PM, Demeestere K et al (2012) TiO_2 mediated heterogeneous photocatalytic degradation of moxifloxacin: operational variables and scavenger study. Appl Catal B 111–112:150–156. https://doi.org/10.1016/j.apcatb.2011.09.029

Vasu D, Karthi Keyan A, Sakthinathan S, Chiu T-W (2022) Investigation of electrocatalytic and photocatalytic ability of Cu/Ni/TiO_2/MWCNTs nanocomposites for detection and degradation of antibiotic drug Furaltadone. Sci Rep 12:886. https://doi.org/10.1038/s41598-022-04890-z

Vivek S, Preethi S, Babu KS (2022) Interfacial effect of mono (Cu, Ni) and bimetallic (Cu–Ni) decorated ZnO nanoparticles on the sunlight assisted photocatalytic activity. Mater Chem Phys 278:125669. https://doi.org/10.1016/J.MATCHEMPHYS.2021.125669

Xia Y, Zhu S, Fu X et al (2022) In situ loading of Ag2S particle on Nb_2O_5 sheets for synergistically enhanced photocatalytic decontamination of methylene blue. J Mater Sci: Mater Electron 33:2125–2137. https://doi.org/10.1007/s10854-021-07419-8

Yan J, Wu G, Guan N, Li L (2014) Nb_2O_5/TiO_2 heterojunctions: synthesis strategy and photocatalytic activity. Appl Catal B 152–153:280–288. https://doi.org/10.1016/J.APCATB.2014.01.049

Yang X, Duan J, Zhang X et al (2022) Heterojunction architecture of Nb_2O_5/g-C3N4 for enhancing photocatalytic activity to degrade organic pollutants and deactivate bacteria in water. Chin Chem Lett 33:3792–3796. https://doi.org/10.1016/j.cclet.2021.11.031

Yin L, Shen Z, Niu J et al (2010) Degradation of pentachlorophenol and 2,4-dichlorophenol by sequential visible-light driven photocatalysis and laccase catalysis. Environ Sci Technol 44:9117–9122. https://doi.org/10.1021/es1025432

Yu W, Du B, Yang L et al (2019) Occurrence, sorption, and transformation of free and conjugated natural steroid estrogens in the environment. Environ Sci Pollut Res 26:9443–9468